European Journal of Pharmaceutics and Biopharmaceutics 137 (2019) 56–67

Contents lists available at ScienceDirect

European Journal of Pharmaceutics and Biopharmaceutics

journal homepage: www.elsevier.com/locate/ejpb

Research paper

Anisamide-targeted PEGylated gold nanoparticles designed to target prostate cancer mediate: Enhanced systemic exposure of siRNA, tumour growth suppression and a synergistic therapeutic response in combination with paclitaxel in mice

Xue Luan[a,1], Kamil Rahme[b,c,1], Zhongcheng Cong[a], Limei Wang[a,e], Yifang Zou[a], Yan He[a], Hao Yang[a], Justin D. Holmes[c,d], Caitriona M. O'Driscoll[f], Jianfeng Guo[a,*]

[a] School of Pharmaceutical Sciences, Jilin University, Changchun 130021, China
[b] Department of Sciences, Faculty of Natural and Applied Science, Notre Dame University (Louaize), Zouk Mosbeh, Lebanon
[c] Department of Chemistry and the Tyndall National Institute, University College Cork, Cork, Ireland
[d] AMBER@CRANN, Trinity College Dublin, Dublin 2, Ireland
[e] Department of Pharmacy, The General Hospital of FAW, Changchun 130011, China
[f] Pharmacodelivery Group, School of Pharmacy, University College Cork, Cork, Ireland

ARTICLE INFO

Keywords:
Non-viral siRNA delivery
Cancer gene therapy
Combination therapy
Prostate cancer

ABSTRACT

Small interfering RNA (siRNA) has recently illustrated therapeutic potential for malignant disorders. However, the clinical application of siRNA-based therapeutics is significantly retarded by the paucity of successful delivery systems. Recently, multifunctional gold nanoparticles (AuNPs) as non-viral delivery carriers have shown promise for transporting chemotherapeutics, proteins/peptides, and genes. In this study, AuNPs capped with polyethylenimine (PEI) and PEGylated anisamide (a ligand known to target the sigma receptor) have been developed to produce a range of positively charged anisamide-targeted PEGylated AuNPs (namely Au-PEI-PEG-AA). The anisamide-targeted AuNPs effectively complexed siRNA *via* electrostatic interaction, and the resultant complex (Au_{110}-PEI-PEG_{5000}-AA.siRNA) illustrated favourable physicochemical characteristics, including particle size, surface charge, and stability. *In vitro*, anisamide-targeted AuNPs selectively bound to human prostate cancer PC-3 cells, inducing efficient endosomal escape of siRNA, and effective downregulation of the *RelA* gene. *In vivo*, prolonged systemic exposure of siRNA was achieved by anisamide-targeted AuNPs resulting in significant tumour growth suppression in a PC3 xenograft mouse model without an increase in toxicity. In addition, a combination of siRNA-mediated NF-κB knockdown using anisamide-targeted AuNPs with Paclitaxel produced a synergistic therapeutic response, thus providing a promising therapeutic strategy for the treatment of prostate cancer.

1. Introduction

Prostate cancer is a leading cause of cancer-related fatalities for male population; in 2018 a total of 1,276,106 new cases and 358,989 deaths from this malignant disorder are forecasted to occur worldwide [1]. Recent advances in understanding the molecular pathology underlying prostate carcinogenesis have provided significant opportunities for the application of gene-based therapeutic strategies [2]. Small interfering RNA (siRNA), which results in sequence-specific post-transcriptional gene silencing in mammalian cell lines, has shown impressive anti-cancer potential [3]. However, the paucity of successful delivery systems dramatically retards the clinical translation of siRNA-based therapeutics for cancer [4].

Recently, the development of novel organic and inorganic materials has revolutionised the field of siRNA delivery for treatment of solid tumours [5–7] and haematopoietic malignancies [8,9]. As a result, a variety of non-viral siRNA delivery nanoparticle (NP) formulations have been developed for prostate cancer therapy [10]. Despite the promise, significant challenges such as inefficient siRNA encapsulation or complexation, *in vitro* and *in vivo* NP instability, non-specific cell

* Corresponding author.
E-mail address: jguo@jlu.edu.cn (J. Guo).
[1] Xue Luan and Kamil Rahme shared first authorship.

https://doi.org/10.1016/j.ejpb.2019.02.013
Received 22 September 2018; Received in revised form 18 December 2018; Accepted 15 February 2019
Available online 16 February 2019
0939-6411/

binding, poor endosomal or lysosomal escape, and low gene knockdown efficacy, remain to be overcome before siRNA-based therapeutics can be widely accepted for use in patients with prostate cancer [10,11].

Among the diverse range of nanoparticulate delivery carriers, gold NPs (AuNPs) have been utilised to develop siRNA nanomedicines mainly due to favourable physicochemical properties [12]. Previously, spherical positively charged AuNPs were synthesised using surfactant-free methods in the presence of L-cysteine methyl ester hydrochloride [$HSCH_2CH(NH_2)COOCH_3{\cdot}HCl$] [13] and poly (ethylenimine) (PEI) [14] as the capping agents, respectively. Although these positively charged AuNPs (Au-L-cysteine and Au-PEI) demonstrated effective gene silencing *in vitro*, activity was curtailed due to non-specific binding to serum proteins [13,14]. When Au-L-cysteine was further modified with polyethylene glycol (PEG), stability in serum-containing medium was improved [15]; however, these PEGylated AuNPs displayed poor cellular uptake due to the "PEG dilemma" phenomenon [16]. Bi-functional PEG moieties on AuNPs have therefore been exploited to facilitate conjugation of targeting ligands, resulting in cell-specific internalisation [17].

Recently, sigma receptors have been found to overexpress in a variety of human cancer cell lines and patient tumour tissues (e.g. prostate carcinoma) [18,19]. Anisamide (AA) is known as a ligand to target the sigma receptors overexpressed on the prostate cancer cell membrane [20,21]. Informed by our previous studies, a range of novel spherical AuNPs were developed in this study for targeted delivery of siRNA in the treatment of prostate cancer. The spherical Au core was initially coated with PEI to achieve a cationic surface (Au-PEI) capable of complexing siRNA and inducing endosomal escape. To enhance stability in physiological environments and mediate selective uptake in prostate cancer cells, Au-PEI was further modified by PEGylated anisamide to generate a PEGylated Au-AA targeted construct, Au-PEI-PEG-AA. The resultant complex of Au-PEI-PEG-AA with siRNA against *RelA* gene (a gene product from the NF-κB transcription factor complex [22]) was investigated alone and in combination with paclitaxel for therapeutic efficacy in a prostate carcinoma xenograft mouse model.

2. Materials and methods

2.1. Materials

PC-3 (human prostate cancer cell line) and CT26 (mouse colon cancer cell line) were purchased from the American Type Culture Collection (ATCC, USA). Negative control siRNA (siNeg) (sense sequence 5′-UUC UCC GAA CGU GUC ACG U-3′, no modification), FAM-labelled siRNA (siFAM) [sense sequence 5′-UUC UCC GAA CGU GUC ACG U-3′, modified by carboxyfluorescein (FAM) on 5′ of sense sequence], and RelA siRNA (siRelA) (sense sequence 5′-CCA UCA ACU AUG AUG AGU U-3′) were purchased from GenePharma Co., Ltd., Shanghai, China. These HPLC-purified siRNAs were prepared in RNase-free water following manufacturer's recommendations.

Tetrachloroauric acid trihydrate ($HAuCl_4{\cdot}3H_2O$), L-ascorbic acid ($C_6H_8O_6$), *N*-(3-Dimethylaminopropyl)-*N*′-ethylcarbodiimide hydrochloride (EDC.HCl), N-hydroxysuccinimide (NHS), *N*,*N*-Diisopropylethylamine (DIPEA) purified by re-distillation, branched PEI solutions (*Mw* = 2 kDa, 50% w/v), *p*-Anisic acid (99.5%), dry dichloromethane (DCM), dry pentane, magnesium sulfate ($MgSO_4$), and thiol PEG Amine (HS-PEG_{7500}-NH_2 and HS-PEG_{3500}-NH_2) were purchased from Sigma-Aldrich. In addition, HS-PEG_{5000}-NH_2 was obtained from PEG Creative Work. All chemicals were used as received without any further purification.

2.2. Synthesis of AuNPs

Purified H_2O (resistivity ≈ 18.2 MΩ cm) was used as a solvent for AuNP synthesis. Glassware was cleaned with aqua regia (3 parts of concentrated HCl and 1 part of concentrated HNO_3), rinsed with distilled water, ethanol and acetone, and dried overnight before use.

2.2.1. Optical spectra

The optical absorption spectra were obtained using the Evolution 60 UV–Visible spectrophotometer with a Xenon Flash Lamp (300–1100 nm range, 0.5 nm resolution) (Thermo Fisher Scientific).

2.2.2. Scanning electron microscopy (SEM)

AuNP samples were deposited onto a Silicon wafer and air-dried prior to analysis using a FEI 630 NanoSEM equipped with an Oxford INCA energy dispersive X-ray (EDX) detector operated at 5 kV.

2.2.3. Nuclear magnetic resonance (NMR)

NMR was recorded in deuterated chloroform ($CDCl_3$) using a Bruker NMR (400 or 300 MHz) at ambient temperature.

2.2.4. Dynamic light scattering (DLS)

Particle size and zeta potential were measured in deionised water (0.2 μm membrane-filtered) using the Malvern Nano-ZS (Malvern Instruments, UK) at 25 °C with the default non-invasive back scattering (NIBS) technique at a detection angle of 173°.

2.2.5. Synthesis of Au-PEI

50 mL of freshly prepared $HAuCl_4{\cdot}3H_2O$ aqueous solution (1 mM) were added into 0.3 mL of PEI aqueous solution (5 mM) at RT. Subsequently, 0.775 mL of L-ascorbic acid (100 mM) was added into the solution and stirred at RT for 3 h, in order to produce Au-PEI with ~110 nm of diameter (Au_{110}-PEI). In addition, the synthesis of Au_{25}-PEI, Au_{60}-PEI and Au_{95}-PEI was described in the Supporting Information.

2.2.6. Synthesis of NHS-activated anisic acid

NHS-activated anisic acid was produced as previously described [14]. Briefly, EDC.HCl (1.5 eq, 1.9 g, 9.9 mmol) was added to the *p*-anisic acid solution (6.572 mmol) in dry DCM (250 mL) under Argon, followed by the addition of NHS (1.45 eq, 1.1 g, 9.56 mmol). The reaction mixture was stirred for ~42 h under Argon at RT. The organic phase was washed twice with water followed by a wash with brine, dried over $MgSO_4$, filtered on Whatman filter paper, and evaporated. The activated ester thus obtained was left to stir in 30 mL of dry pentane for ~48 h, filtered, dried under vacuum, and used without further purification. The yield of the anisic-NHS ester (AA-NHS) was approximately 90%. The product was analysed using NMR spectroscopy [(400 MHz, $CDCl_3$): δ ppm 8.08–8.11 (d, 2H, ArH-CO-), 6.97–6.99 (d, 2H, ArH-OCH_3), 3.89 (s, 3H, OCH_3), 2.91 (s, 4H CH_2-CH_2 in NHS ring)] [14].

2.2.7. Synthesis of PEGylated anisamide (SH-PEG_{5000}-AA)

100 mg of SH-PEG_{5000}-NH2 (0.02 mmol) were dried under the vacuum for 10 min at RT, followed by the application of a flow of nitrogen (N_2), and further dried under the vacuum for 5 min at RT. The SH-PEG_{5000}-NH_2 powder were then dissolved in 4 mL of DCM under N_2 and 2 mL of AA-NHS (0.034 mmol) in dry DCM was added and stirred at 0 °C. Subsequently, 50 μL of DIPEA (0.615 mmol) in dry DCM was added and stirred under N_2 at RT for 48 h. The resultant SH-PEG_{5000}-AA was precipitated at 0 °C using 100 mL cold diethyl ether/ethanol solution (v/v = 99/1). The SH-PEG_{5000}-AA was collected at 0 °C by centrifugation at 11,000 rpm and dried overnight under the vacuum. The SH-PEG_{5000}-AA (~90% yield) was characterised by NMR in $CDCl_3$: δ ppm 7.79–7.81 (d, 2H, ArH-CO-), 6.90–6.92 (d, 2H, ArH-OMethyl), 3.85 (s, Ar-OCH_3), 3.65 (O-CH_2-CH_2 of PEG), 2.9 (CH_2-C = O). The degree of anisamide attachment was ~100% as calculated from the peak integration ratio of phenyl proton at δ 7.78 to methylene protons at δ 3.65. In addition, the synthesis of SH-PEG_{3500}-AA and SH-PEG_{7500}-AA was described in the Supporting Information.

2.2.8. Pegylation of Au-PEI (Au-PEI-PEG and Au-PEI-PEG-AA)

The Au-PEI was PEGylated by adding SH-PEG-NH_2 (100 μM) or SH-PEG-AA (100 μM), in which the final concentrations were fixed approximately at a molar ratio of 1:250 for SH-PEG-NH_2/SH-PEG-AA and $HAuCl_4$ (Fig. S4). This reaction was continued with stirring for ~6 to 16 h at RT. The resultant Au-PEI-PEG and Au-PEI-PEG-AA were collected by centrifugation at 11,000 rpm for 5 min. As a result, ~60% of the initial SH-PEG-NH_2 and SH-PEG-AA were conjugated onto the Au surface, this was confirmed using UV–vis spectroscopy (Fig. S5). In addition, the successful PEGylation was confirmed using DLS and SEM.

2.3. Cytotoxicity

PC-3 and CT26 cells were maintained in RPMI-1640 medium (CORNING) supplemented with 10% FBS and a Penicillin-Streptomycin Nystatin solution (Biological Industries). Five thousand PC-3 or CT26 cells were seeded per well in 96-well culture plates. After 24 h, AuNPs (concentrations = 1, 5, 10, 20, 50, 100, 250, 500 and 1000 μg/mL) were added to the cells for 72 h under normal growth conditions. Following incubation, cells were incubated with 20 μL 3-(4,5-dimethylthiazol-2-yl)-2, 5-diphenyltetrazolium bromide (MTT) stock (5 mg/mL in PBS) in 200 μL fresh growth medium for 4 h at 37 °C. ~100 to 200 μL DMSO was added to dissolve the purple formazan products. The results were read at 570 nm using a microplate reader.

2.4. Preparation and physicochemical characterisation of AuNP.siRNA complexes

Solutions of Au-PEI, Au-PEI-PEG, and Au-PEI-PEG-AA (1 μg/μL) were added to siRNA solutions at different weight ratios (WRs) of AuNPs to siRNA, followed by 2 h sonication at 55–60 °C. The efficiency of AuNPs to complex siRNA was assessed using gel retardation assay [17]. Briefly, solutions of AuNPs and siRNA (0.2 μg siNeg) at various WRs were loaded onto 1% (w/v) agarose gels in Tris-Borate-EDTA (TBE) buffer containing the GelStain (Transgen Biotech, China). Electrophoresis was performed at 90 V for 20 min and the resultant gels were photographed under UV.

Measurements of particle size and zeta potential of AuNP.siRNA complexes were performed as described in Section 2.2.4. The concentration of siRNA was fixed at 1 μg/mL.

Complexes containing 0.2 μg siNeg at WR40 were incubated for 1, 2, 4 and 8 h in 50% (v/v) fetal bovine serum (FBS; Gibco) at 37 °C. After incubation, samples were heated for 5 min at 80 °C for serum inactivation. Samples were then treated with excess heparin (1000 IU/mL) at RT for 1 h to release siRNA from AuNPs. Samples were loaded onto 1.5% (w/v) agarose gels containing the GelStain. Electrophoresis was performed at 90 V for 20 min and the resultant gels were photographed under UV.

In addition, complexes (WR40) were incubated in 50% (v/v) FBS at 37 °C for 24 h, and the particle sizes were measured using Malvern Nano-ZS as described in Section 2.2.4. FBS alone and complexes incubated in deionised water at 37 °C for 24 h were used as controls. The concentration of siRNA was fixed at 1 μg/mL.

2.5. Cellular uptake

PC-3 and CT26 cells were respectively seeded at 1×10^5 cells per well in 24-well culture plates one day before transfection. Cells were subsequently treated with AuNPs complexes (WR40) containing 50 nM siFAM and incubated for 8 h under normal growth conditions. Following incubation, cells were washed twice with PBS and trypsinised. After 1000 rpm centrifugation for 5 min, the supernatant was discarded and cells were re-suspended in 1000 μL ice-cold PBS. 10,000 cells were measured for each sample according to the Becton Dickinson FACS-calibur manual.

2.6. Intracellular trafficking

PC-3 cells (1×10^5 cells per well) were seeded in 6-well culture plates with glass bottoms (JET BIOFIL®, China) for 24 h. Cells were subsequently treated with Au-PEI-PEG-AA complexes (WR40) containing 50 nM siFAM and incubated for 4 h under the normal growth conditions. Following this, cells were incubated in LysoTracker® Deep Red (75 nM; Invitrogen) at 37 °C for 30 min. Fresh growth medium was added to the cells prior to confocal microscopic analysis using an Olympus FV 1000 microscope.

2.7. Gene knockdown

PC-3 cells (1×10^5 cells per well) were seeded in 24-well culture plates. Following 24 h incubation, cells were transfected by the Au-PEI-PEG-AA formulation (WR40) containing 100 nM siRelA for 24 h. After this, total RNA was isolated from cells using TransZol UP (Transgen Biotech, China). First-strand cDNA was generated from total RNA samples using TransScript® All-in-One First-Strand cDNA Synthesis SuperMix for qPCR (Transgen Biotech, China). Gene expression was assessed by real-time quantitative PCR (qPCR) using TransStart® Top Green qPCR SuperMix (Transgen Biotech, China). Assays were carried out using primers for RelA (forward: 5′-GCC TCA TCC ACA TGA ACT TGT GGG-3′; reverse: 5′-ACC ATG GTC TGG GCA AGG ACT GGG-3′) and GAPDH (forward: 5′-ACC ACA GTC CAT GCC ATC AC-3′; reverse: 5′-TCC ACC ACC CCC TGT TGC TGT A-3′). Amplification was carried out under 40 cycles of denaturation at 94 °C (5 s) and annealing at 60 °C (30 s) (StepOnePlus™ Real-Time PCR System, Applied Biosystems™). The quantitative level of each RelA mRNA was measured as a fluorescent signal corrected according to the signal for GAPDH mRNA.

In addition, PC-3 cells (1×10^5 cells per well) were seeded in 24-well culture plates. Following 24 h incubation, cells were transfected by Au-PEI-PEG-AA formulation (WR40) containing 100 nM siRelA for 48 h. Subsequently, cells were lysed using RIPA buffer [50 mM Trish (pH 7.4), 150 mM NaCl, 1% NP-40, 0.5% sodium deoxycholate, 1% SDS, sodium orthovanadate, sodium fluoride, EDTA, and leupeptin], and protein concentrations were quantified using the Easy II BCA Protein Quantitative Kit (GenStar, China). ~30–50 μg of proteins per sample were loaded onto an SDS-PAGE and electrophoresed at 80 V for 0.5 h and subsequently at 120 V for 1.5 h. Proteins were then transferred to a PVDF membrane (Immobilon®-P Transfer Membrane; Millipore) at 200 mA for 1.5 h. Membranes were incubated with appropriate antibodies [RelA (#1574i53) and β-actin (#8427f55), purchased from Affinity, USA] at RT for 12 h. Antibody reactive bands were detected using MicroChemi (DNR Bio-Imaging Systems Ltd., Israel). Densitometry analysis of bands was performed using ImageJ, and all results were normalised to the β-actin control.

2.8. In vitro anti-cancer effects

PC-3 cells (100,000 per well) were seeded in 24-well culture plates for one day. Au-PEI-PEG-AA complexes (WR40) containing 100 nM siRelA were applied to the cells for 24 h. Cells were subsequently incubated with Annexin V-FITC and propidium iodide (PI) supplied from TransDetect® Annexin V-FITC/PI Cell Apoptosis Detection Kit (Transgen Biotech, China). The apoptotic cells were analysed using flow cytometry (Becton Dickinson FACS-calibur).

PC-3 cells (5000 per well) were seeded in 96-well culture plates. After 24 h, Au-PEI-PEG-AA complexes (WR40) containing 100 nM siRelA were added to cells and incubated for 48 and 72 h. Following incubation, cells were treated with the TransDetect® Cell Counting Kit (CCK) (Transgen Biotech, China) and incubated for 2 h before measuring the absorbance at 450 nm.

In addition, PC-3 cells (5000 per well) were seeded in 96-well culture plates. After 24 h, Au-PEI-PEG-AA complexes (WR40) containing 100 nM siRelA were added to cells and incubated for 4 h. After this,

cells were further treated with Paclitaxel (PTX, purchased from Hainan Choitec Pharmaceuticals Co., Ltd.; [c] = 50, 100 and 200 nM) for 20 h. Following incubation, cells were treated with the TransDetect® Cell Counting Kit (CCK) solution (Transgen Biotech, China) and incubated for 2 h before measuring the absorbance at 450 nm.

2.9. Animal experiments

The animal ethics committee of Jilin University approved all experiments. All mice were maintained in a pathogen free animal facility for at least 2 weeks before the experiments.

2.10. In vivo toxic studies

Male BALB/C mice (6–8 weeks) were purchased from Changchun Institute of Biological Products, China. Animals (n = 4 per group) were intravenously injected with the siNeg (~1 mg/kg) complexed with Au-PEI-PEG or Au-PEI-PEG-AA (WR40), 100 μL of saline (negative control) and 100 μg of poly polyinosinic:polycytidylic acid [poly (I:C)] (positive control) through the mouse tail vein. Blood samples were collected at 2 h post injection. Serum IFN-α was measured by the IFN alpha Mouse ELISA Kit (Invitrogen).

In addition, mice (n = 4 per group) were intravenously injected with Au-PEI-PEG-AA formulations (WR40) containing siRelA (~1 mg/kg) at Day 1, 3, 5, 7 and 9. After 4 h, animals were treated with intraperitoneal (i.p.) injection of PTX (~10 mg/kg). The body weight of mice was recorded regularly. On the endpoint (Day 14), major tissues (the heart, liver, spleen, lung and kidney) were collected and analysed using the haematoxylin and eosin (H & E) staining assay. In addition, blood samples were collected and analysed using a haemacytometer, in order to determine the haematological toxicity.

2.11. Pharmacokinetics

Male BALB/C mice (~20–22 g) (n = 4 per group) were intravenously injected with siFAM either alone (~1 mg/kg) or complexed with Au-PEI-PEG or Au-PEI-PEG-AA (WR40). Blood samples (~30 μL) were collected at 1, 3, 5, 10, 15, 30 and 60 min. The extraction and quantification of siFAM were carried out as described in [23]. The extraction efficiency of siFAM from Au-PEI-PEG and Au-PEI-PEG-AA was 94% and 96% respectively. The concentration of siFAM in plasma obtained from standard curves was corrected using these determined extraction efficiencies. Pharmacokinetic parameters were calculated using DAS 2.0.

2.12. Tissue distribution

The xenograft model was established by subcutaneous injection of 5×10^6 PC-3 cells into the flank of male BALB/c nude mice (5–6 weeks, purchased from Beijing Vital River Laboratory Animal Technology Co., Ltd.). Tumour growth was recorded regularly, and the volume was calculated using a formula $a^2b(\pi/6)$, where a is the minor diameter of the tumour and b is the major diameter perpendicular to diameter a. When the volume reached ~250 mm^3, siFAM either alone (~1 mg/kg) or formulated with Au-PEI-PEG or Au-PEI-PEG-AA was intravenously injected into tumour bearing mice (n = 4 per group). Two hours post treatment, mice were sacrificed, and the organs (heart, liver, spleen, lung and kidneys) and tumours were collected. As described in [24], the liver was homogenised in 1 mL lysis buffer, and other tissues were homogenised in 300 μL lysis buffer. The homogenised samples were incubated at 65 °C for 10 min. siFAM in the supernatant was extracted and measured as described in Section 2.11. The dose of siRNA accumulated in tissues was quantified from a strand curve obtained by spiking known amounts of siFAM alone or siFAM complexed with AuNPs in tissues from untreated mice [24].

2.13. In vivo anti-tumour study

When the tumour volume reached ~150 mm^3, siRelA (~1 mg/kg) formulated with Au-PEI-PEG-AA was intravenously injected into animals (n = 4 per group) at Day 1, 3 and 5. Four hours post-injection, PTX was intraperitoneally injected at a dose of ~10 mg/kg into the tumour bearing mice. Tumour growth and body weight were recorded regularly, and the tumour volume was calculated as described above. Treatments of saline, PTX alone and siNeg (~1 mg/kg) formulated with Au-PEI-PEG-AA were used as controls.

2.14. Statistical analysis

Data were calculated as the mean ± standard deviation (SD). An unpaired Student's *t*-test (two-tailed) was used to test the significance of differences between two mean values. A one-way ANOVA (Bonferroni's Post-Hoc test) was used to test the significance of differences in three or more groups. In addition, a two-way ANOVA (Bonferroni's Post-Hoc test) was used to test the significance of differences in measurements of body weight, pharmacokinetics, and tumour growth. In all experiments, $p < 0.05$ was considered statistically significant.

3. Results

3.1. Synthesis and physicochemical characterisation of Au-PEI and anisamide target gold NPs (Au-PEI-PEG-AA)

Au-PEI NPs with a range of particle sizes namely; Au_{25}-PEI, Au_{60}-PEI, Au_{95}-PEI and Au_{110}-PEI, were synthesised by the conjugation of PEI onto the surface of AuNPs. As previously reported [14], AuNPs were initially modified with branched PEI (*Mw* = 2 kDa) to achieve positively charged Au-PEI. It has been reported that PEI with high *Mw* (e.g. > 10 kDa) can generate higher transfection efficiency relative to low *Mw* PEI (e.g. 2 kDa) [25]. However, low *Mw* PEI is less toxic and more biocompatible compared to high *Mw* PEI [26]. Consequently, PEI 2 kDa was to chosen to bind siRNA to the AuNPs (see Section 3.3) and to facilitate intracellular release (see Section 3.4.2).

Conjugation was confirmed by UV–vis spectroscopy indicating that a red shift of ~50 nm accompanied by peak broadening which was clearly observed when the particle size increased from ~25 to 100 nm (Fig. 1a). The Au_{110}-PEI presented a spherical shape with a diameter of ~110 nm (Fig. 1b). The Au_{25}-PEI, Au_{60}-PEI and Au_{95}-PEI demonstrated similar morphology with diameters of ~25, 60 and 95 nm, respectively (Fig. S1). In contrast to SEM results, the particle size of Au-PEI obtained from the DLS was slightly larger (Fig. 1c and Table S1), indicating that the AuNPs were successfully coated with PEI. In addition, the positive surface charge of the Au-PEI gradually decreased as the particle size of the AuNPs increased (Fig. 1d and Table S1).

The anisic acid was activated by reacting with NHS to form an anisic-NHS ester (AA-NHS), which was confirmed using NMR (Fig. S2) [14]. The AA-NHS reacted with the amino group ($-NH_2$) of SH-PEG-NH_2 to form a stable amide linkage, producing SH-PEG-AA (Fig. S3). The Au-PEI was subsequently chemically modified with SH-PEG-AA to form cationic anisamide-targeted PEGylated AuNPs (Au-PEI-PEG-AA). Results in Fig. 2a indicate that the particle size of Au-PEI-PEG-AA with the same core size (e.g. Au_{110}-PEI) was clearly increased with the PEG *Mw* (Table S1). In contrast, the zeta potential of Au-PEI-PEG-AA with the same core size (e.g. Au_{110}-PEI) was gradually decreased with increasing the PEG *Mw* (Fig. 2b and Table S1). In addition, a thin 'halo-like' layer was clearly observed on the surface of Au-PEI-PEG-AA (Fig. 2c), most likely due to the attachment of PEG chains. In summary, these results show that the PEGylated anisamide was successfully conjugated to the surface of Au-PEI.

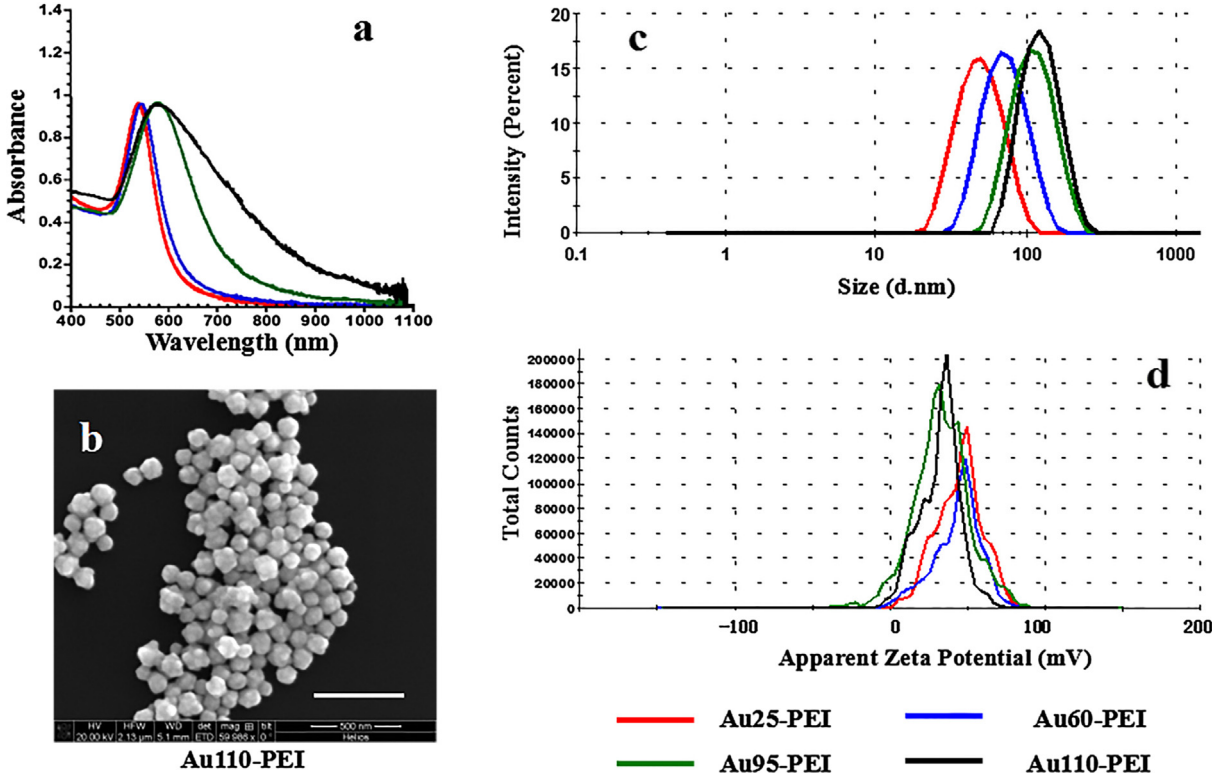

Fig. 1. (a) UV–vis spectrum of the Au-PEI NPs. (b) SEM image of Au_{110}-PEI (scale bar = 500 nm). (c) Particle size and (d) zeta potential of Au_{25}-PEI, Au_{60}-PEI, Au_{95}-PEI, Au_{110}-PEI obtained using the Malvern Nano-ZS.

3.2. Cytotoxicity of Au-PEI-PEG and anisamide target gold NPs (Au-PEI-PEG-AA)

The *in vitro* toxicity of Au-PEI-PEG and Au-PEI-PEG-AA was assessed using human prostate cancer PC-3 cells (Table S2). Results show that the attachment of PEG with increasing *Mw* to AuNPs with the same core size (e.g. Au_{110}-PEI) significantly enhanced cell viability; for example, IC50 values of Au_{110}-PEI-PEG_{3500}-AA, Au_{110}-PEI-PEG_{5000}-AA and Au_{110}-PEI-PEG_{7500}-AA in PC-3 cells were approximately 390, 440 and 500 μg/mL respectively. In addition, the cytotoxicity of AuNPs with the same PEG length was significantly reduced when the particle size was increased; for instance, IC50 values of Au_{25}-PEI-PEG_{5000}-AA, Au_{60}-PEI-PEG_{5000}-AA, Au_{95}-PEI-PEG_{5000}-AA and Au_{110}-PEI-PEG_{5000}-AA in PC-3 cells were approximately 100, 200, 330 and 440 μg/mL respectively. Similar IC50 values were also recorded for AuNPs in CT26 cells (data not shown).

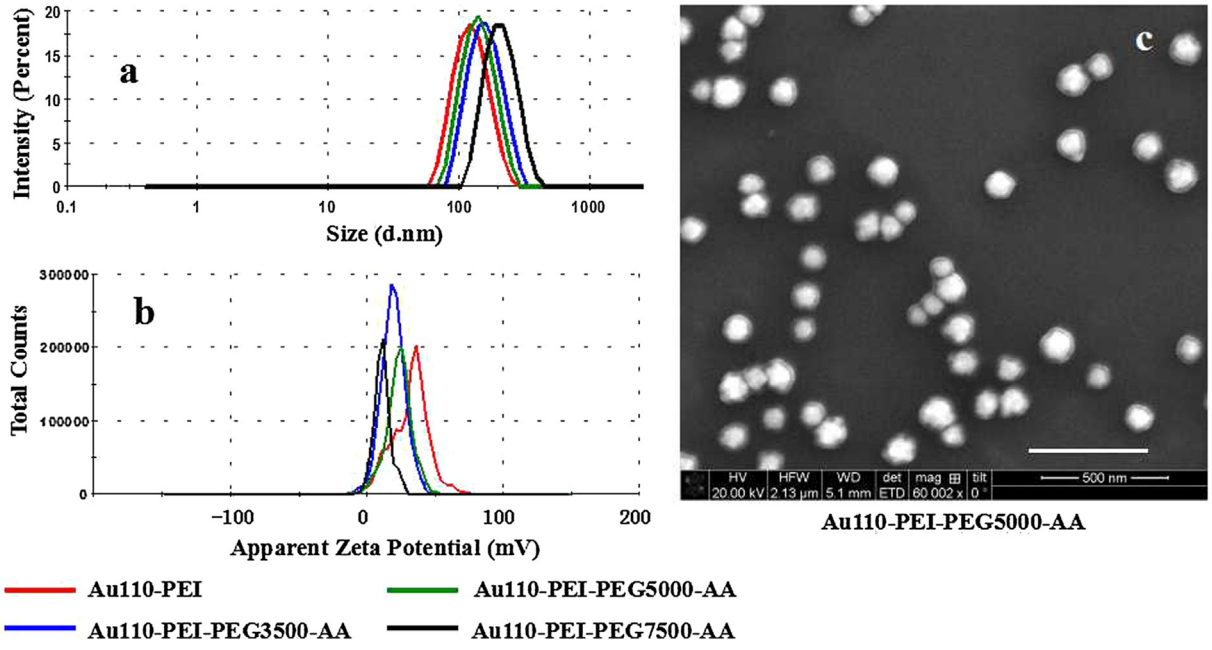

Fig. 2. (a) Particle size and (b) zeta potential of Au_{110}-PEI, Au_{110}-PEI-PEG_{3500}-AA, Au_{110}-PEI-PEG_{5000}-AA, and Au_{110}-PEI-PEG_{7500}-AA Au_{95}-PEI obtained using the Malvern Nano-ZS. (c) SEM image of Au_{110}-PEI-PEG_{5000}-AA (scale bar = 500 nm).

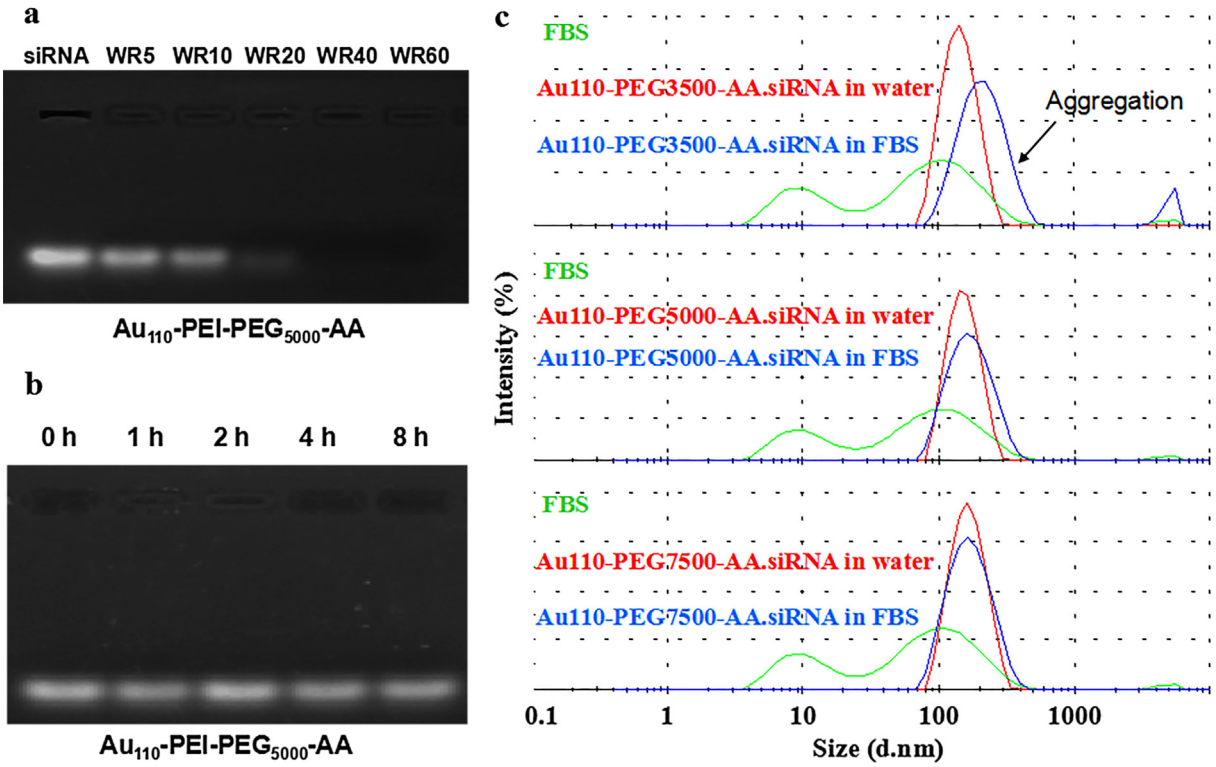

Fig. 3. (a) Complexation of siRNA (0.25 μg) with Au_{110}-PEI-PEG_{5000}-AA at weight ratios (WRs) of 5, 10, 20, 40 and 60. (b) Stability of siRNA (0.25 μg) complexed with Au_{110}-PEI-PEG_{5000}-AA at WR40 following incubation for 0, 1, 2, 4 and 8 h in 50% FBS-containing medium at 37 °C. (c) Aggregation of AuNP.siRNA formulations (WR40) incubated in 50% FBS-containing medium at 37 °C for 24 h. Size distribution of FBS alone and formulations in deionised water were used as controls.

It is interesting to note that anisamide-targeted AuNPs demonstrated slightly higher ($p > 0.05$) PC-3 cell death compared to non-targeted counterparts (Table S2). In contrast, no significant difference in cytotoxicity was found between Au-PEI-PEG and Au-PEI-PEG-AA in CT26 cells (a cell line where the sigma receptor is less well expressed [27]) (data not shown). Therefore, these results suggest that the cytotoxic profiles of Au-PEI-PEG-AA may be dependent on the density of sigma receptors in cell lines (see Section 3.4.1).

On the basis of the cytotoxicity results, the concentrations of Au-PEI-PEG and Au-PEI-PEG-AA used for the following *in vitro* experiments ensured > 90% of cell viability.

3.3. Complexation of siRNA with Au-PEI-PEG and Au-PEI-PEG-AA

The formation of AuNP and siRNA complexes *via* the electrostatic interaction between cationic PEI and anionic siRNA was assessed using a gel retardation assay (Fig. 3a, S6, S7 and S8). Results show that full binding of siRNA with Au_{110}-PEI-PEG_{5000} and Au_{110}-PEI-PEG_{5000}-AA was achieved from WR40 of AuNPs and siRNA onwards (Figs. 3a and S8). However, the AuNPs with smaller diameters did not bind siRNA as efficiently as the bigger counterparts (Fig. S7), most likely due to the fact that the bigger Au core, particularly with the spherical shape, may provide more binding space for small nucleic acids (e.g. siRNA) with a stiff rod-like structure. In addition, it is interesting to note that AuNPs with shorter PEGylation (*Mw* = 3500 kDa) achieved full complexation with siRNA at WR20 onwards, but full binding of siRNA was achieved only from WR40 onwards by AuNPs with longer PEGylation (*Mw* = 5000 and 7500 kDa) (Fig. S8). As the AuNPs are modified with the same grafting density (i.e. ~60%, Fig. S5), a possible explanation is that the PEG with the higher *Mw* (proportional to the chain length) on the Au surface may fold back and overlap each other thus negatively affecting the siRNA binding efficiency.

In addition, the ability of Au-PEI-PEG-AA to protect siRNA from serum nucleases was evaluated in 50% FBS-containing medium at 37 °C (Fig. 3b). Unlike the naked siRNA which degraded significantly after 1 h incubation (data not shown), the siRNA formulated with Au_{110}-PEI-PEG_{5000}-AA (WR40) was resistant to serum degradation up to 8 h. In addition, following incubation in 50% FBS-containing medium at 37 °C, the Au_{110}-PEI-PEG_{3500}-AA.siRNA formulation aggregated at WR40, in contrast the AuNP formulations (WR40) with longer PEG chains (*Mw* = 5000 and 7500 kDa) significantly inhibited the binding of serum proteins (Fig. 3c).

Based on these physicochemical characteristics (Figs. 3, S6–S8), the Au_{110}-PEI-PEG_{5000}-AA.siRNA formulation (WR40) was used for all further *in vitro* and *in vivo* experiments.

3.4. In vitro mechanistic studies using AuNP.siRNA complexes

3.4.1. Cellular uptake

The selective cellular uptake of FAM labelled siRNA (siFAM) complexed with Au_{110}-PEI-PEG_{5000} or Au_{110}-PEI-PEG_{5000}-AA (WR40, 50 nM siRNA) was investigated in both PC-3 (a sigma receptor overexpressing cell line [21]) and CT26 (a cell line where the sigma receptor is less well expressed [27]). As shown in Fig. 4a, Au_{110}-PEI-PEG_{5000}-AA significantly enhanced the uptake of siRNA into PC-3 cells (~45%) compared to the untargeted Au_{110}-PEI-PEG_{5000} (~15%). In the case of CT26 cells cellular uptake by Au_{110}-PEI-PEG_{5000}-AA was significantly reduced (~20%) and was only slightly higher than that obtained by Au_{110}-PEI-PEG_{5000} (~15%) (Fig. 4a). These results indicate that the anisamide-targeted AuNP.siRNA construct has an increased binding affinity for PC-3 cells suggesting the cellular uptake is principally mediated *via* the sigma receptor.

3.4.2. Intracellular trafficking

The intracellular trafficking of anisamide-targeted AuNPs was studied in PC-3 cells using FAM-labelled siRNA (Fig. 4b). After 4 h incubation with Au_{110}-PEI-PEG_{5000}-AA.siFAM (WR40, 50 nM siRNA), fluorescence (green) was detected inside the cells, mainly in the

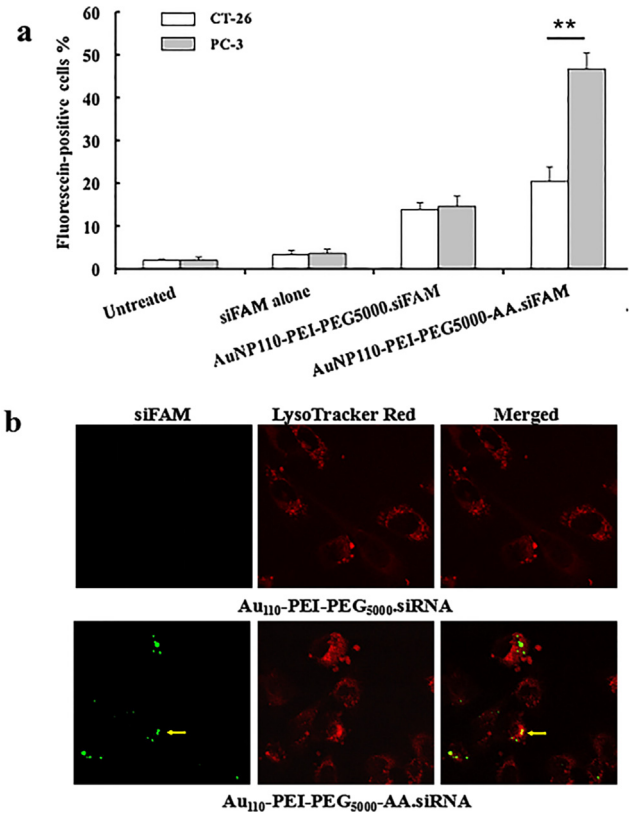

Fig. 4. (a) Fluorescein-positive PC-3 and CT26 cells (%, mean ± SD) after 8 h transfection with Au_{110}-PEI-PEG_{5000}-AA.siFAM (WR40, 50 nM siRNA) ($^{**}p < 0.01$). (b) Intracellular trafficking of Au_{110}-PEI-PEG_{5000}-AA.siFAM (WR40, 50 nM siRNA) in PC-3 cells at 4 h post-transfection using confocal microscopy. Only the minority of FAM-labelled siRNA was co-localised with LysoTracker Red (as indicated by yellow arrows). (For interpretation of the references to colour in this figure legend, the reader is referred to the web version of this article.)

cytoplasm and without co-localisation with the lysosomal marker (red) (Fig. 4b). These results indicate that Au_{110}-PEI-PEG_{5000}-AA achieved efficient endosomal escape of sRNA within 4 h, most likely due to the PEI-mediated "proton sponge effect"; these results are similar to those previously reported for other PEI-modified AuNPs [14,17].

3.4.3. Gene knockdown

The endogenous gene silencing of anti-RelA siRNA (100 nM) using anisamide-targeted AuNPs (WR40) was studied in PC-3 cells (Fig. 5). Following 24 h incubation, siRelA formulated with Au_{110}-PEI-PEG_{5000}-AA significantly ($p < 0.01$) reduced the RelA mRNA level relative to negative controls including naked siRelA, siRelA formulated with Au_{110}-PEI-PEG_{5000}, and siNeg formulated with Au_{110}-PEI-PEG_{5000}-AA (Fig. 5a). In addition, siRelA formulated with Au_{110}-PEI-PEG_{5000}-AA also significantly ($p < 0.01$) down-regulated RelA protein expression after 48 h incubation relative to the aforementioned negative controls (Figs. 5b and S9). It is worth noting that siRelA formulated with Au_{110}-PEI-PEG_{5000}-AA resulted in significantly ($p < 0.05$) greater gene silencing compared to Lipofectamine® 2000 (a commercially available lipid-based transfection reagent used as a positive control in this study) (Figs. 5 and S9), indicating the therapeutic potential of the Au_{110}-PEI-PEG_{5000}-AA construct as a nanoparticulate siRNA delivery system for prostate cancer.

3.4.4. In vitro anti-cancer efficacy

Following efficient NF-κB knockdown, the anisamide-targeted formulation (WR40, 100 nM siRelA) induced significant levels of apoptosis

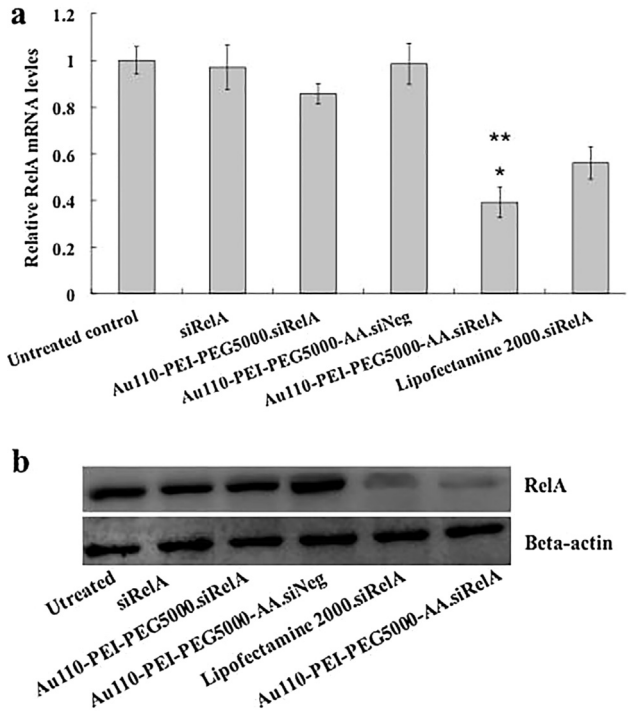

Fig. 5. (a) RelA mRNA downregulation at 24 h post-transfection with Au_{110}-PEI-PEG_{5000}-AA.siRelA (WR40, 100 nM siRNA) in PC-3 cells. (b) RelA protein downregulation at 48 h post-transfection with Au_{110}-PEI-PEG_{5000}-AA.siRelA (WR40, 100 nM siRNA) in PC-3 cells. ($^{*}p < 0.05$ relative to Lipofectamine 2000.siRelA; $^{**}p < 0.01$ relative to Au_{110}-PEI-PEG_{5000}-AA.siNeg).

in PC-3 cells ($p < 0.01$, 24 h incubation) compared to negative controls (Fig. 6a). Due to the apoptotic effects, Au_{110}-PEI-PEG_{5000}-AA.-siRelA significantly slowed down the proliferation of PC-3 cells ($p < 0.01$; ~40% and 60% reductions after 48 h and 72 h incubation, respectively); in contrast, no significant anti-proliferative effect was observed with the negative controls (Fig. 6b). These results suggest that the anti-cancer effects of the AuNPs are related to *RelA* gene silencing, and are not due to cell death or cytotoxicity.

In addition, when combined with Paclitaxel (PTX, an alkaloid with microtubule-targeting capacity, widely utilised to treat a variety of cancers [28]), the downregulation of NF-κB mediated by siRelA using Au_{110}-PEI-PEG_{5000}-AA achieved a synergistic anti-proliferative effect in comparison to either PTX or Au_{110}-PEI-PEG_{5000}-AA.siRNA alone (Fig. S10), indicating the therapeutic potential of this combination strategy in the treatment of prostate cancer.

3.5. In vivo studies using AuNP.siRNA complexes

3.5.1. Toxicity

The *in vivo* toxicity of AuNPs was assessed using mice (n = 4 mice per group) (Figs. S11–S13; Table S3). It has been reported that the immunostimulatory activity of siRNA is dependent on the nucleotide sequence and/or delivery vector type [29]. The nullification of the siRNA-mediated immune response can be achieved by introducing modifications (e.g. 2′-*O*-methyl) in the nucleotides and/or backbone while maintaining silencing activity [30]. In this study, two hours post a single bolus dose of AuNP.siRNA formulations (WR40, ~1 mg/kg siRNA) no increase in interferon alpha (IFN-α) levels were detected (Fig. S11), implying that the immunostimulatory effect of siRNA may be inactivated by targeted delivery using anisamide-targeted AuNPs.

In addition, following treatment with either i.p. injection of Paclitaxel (PTX, ~10 mg/kg) alone, or intravenous (i.v.) injection of Au_{110}-PEI-PEG_{5000}-AA.siRelA (WR40, ~1 mg/kg siRNA) alone, or a combination of PTX (i.p.) and AuNPs (i.v.), no significant decrease in

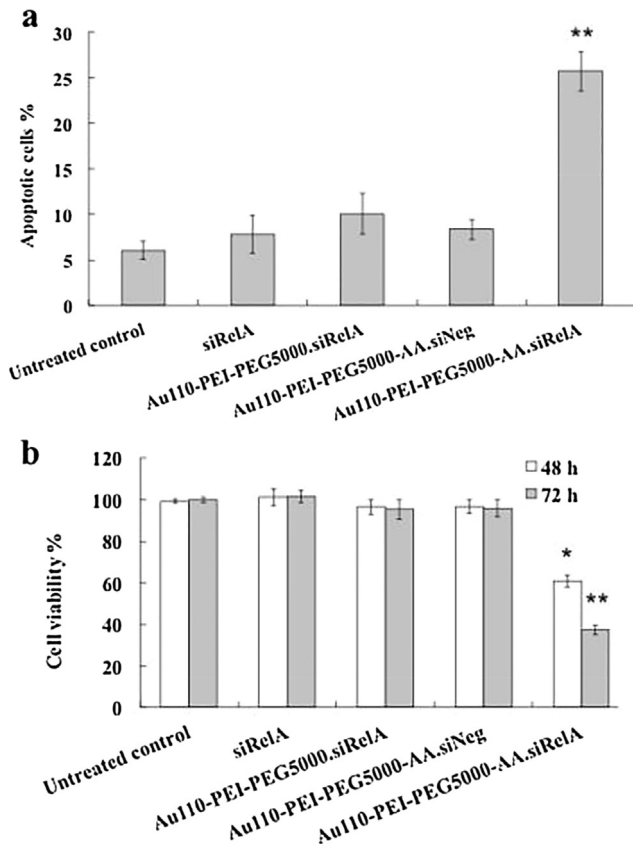

Fig. 6. (a) Apoptotic PC-3 cells (%, mean ± SD) were measured using Annexin V-FITC/PI Cell Apoptosis Detection Kit after 24 h transfection with Au_{110}-PEI-PEG_{5000}-AA.siRelA (WR40, 100 nM siRNA) ($^{**}p < 0.01$ relative to Au_{110}-PEI-PEG_{5000}-AA.siNeg). (b) Cell viability measured in PC-3 cells after 48 and 72 h transfection of Au_{110}-PEI-PEG_{5000}-AA.siRelA (WR40, 100 nM siRNA) using TransDetect® Cell Counting Kit (CCK). ($^{*}p < 0.05$ and $^{**}p < 0.01$ relative to Au_{110}-PEI-PEG_{5000}-AA.siNeg).

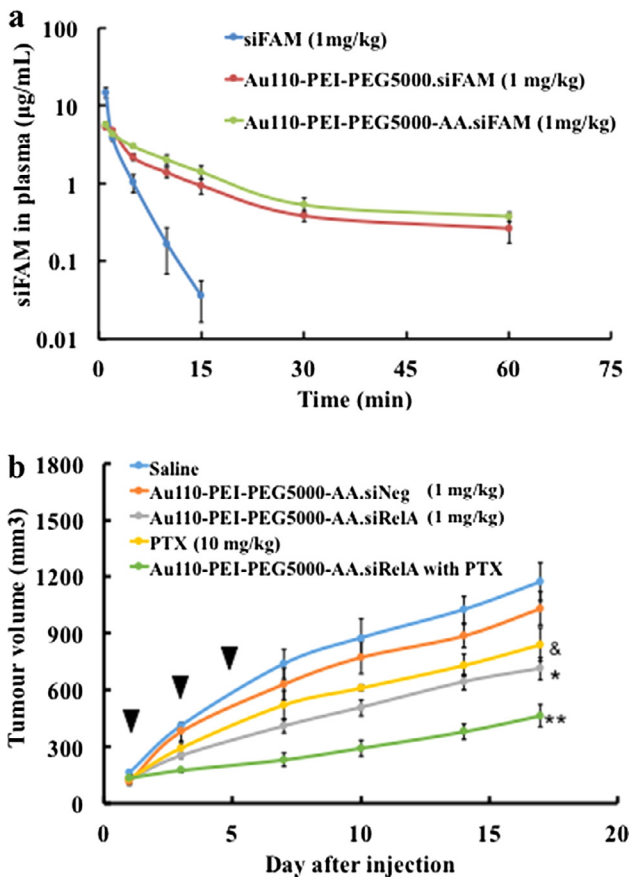

Fig. 7. (a) Plasma concentration of naked siFAM (~1 mg/kg) and siFAM complexed with Au_{110}-PEI-PEG_{5000} or Au_{110}-PEI-PEG_{5000}-AA (WR40) following a single intravenous injection through the mouse tail vein. The concentration of siFAM was plotted using a semi-logarithmic scale (mean ± SD, n = 4). (b) PC-3 xenograft tumour growth reduction (mean ± SD, n = 4) following treatment with anti-RelA siRNA (~1 mg/kg) in different formulations (WR40) with or without Paclitaxel on Day 1, 3 and 5. ($^{\&}p < 0.05$ relative to saline; $^{*}p < 0.05$ relative to targeted formulation containing siNeg; $^{**}p < 0.01$ relative to either Paclitaxel or targeted formulation containing siRelA).

body weight was detected over a 2 week period compared to the saline control group (Fig. S12). At the endpoint (Day 14), the heart, liver, spleen, lung and kidneys were collected and analysed using H & E staining. No significant histological differences between samples from mice treated with PTX, AuNP.siRNA or the combination versus the saline control group were detected (Fig. S13). In addition, the peripheral blood was analysed using the haemacytometer to further examine systemic toxicity (Table S3); the results indicate no significant ($p > 0.05$) haematological toxicity following the treatments when compared to the saline control. In summary, these preliminary murine toxicology studies on the Au_{110}-PEI-PEG_{5000}-AA.siRNA formulation (WR40) indicate no significant signs of systemic toxicity.

3.5.2. Pharmacokinetics

The plasma concentrations versus time for siFAM alone (~1 mg/kg) and siFAM complexed with Au_{110}-PEI-PEG_{5000} or Au_{110}-PEI-PEG_{5000}-AA (WR40) (n = 4 mice per group) are shown in Fig. 7a. Plasma concentrations of free siRNA decreased rapidly, with only residual levels detected less than 15 min post administration. In contrast, the siRNAs complexed with PEGylated AuNPs were more slowly cleared from the plasma, over 60 min post administration (Fig. 7a).

The pharmacokinetic parameters were generated by fitting to a one-compartmental model (Table 1). The rank order in systemic exposure (area under the curve, AUC) was Au_{110}-PEI-PEG_{5000}-AA.siFAM ≈ Au_{110}-PEI-PEG_{5000}.siFAM > siFAM, where the AUC values calculated for AuNP.siRNA formulations were significantly ($p < 0.05$) higher than free siFAM. In addition, PEGylated formulations significantly ($p < 0.05$) reduced clearance (CL) values compared to free siFAM, no significant difference was observed between targeted and non-targeted formulations (Table 1). Corresponding with a decrease in CL, a trend towards longer circulating time (i.e. the half-life, $t_{1/2}$) was observed with a rank order of Au_{110}-PEI-PEG_{5000}-AA.siFAM > Au_{110}-PEI-PEG_{5000}.siFAM > siFAM, where the $t_{1/2}$ value of Au_{110}-PEI-PEG_{5000}-AA.siFAM (6.20 min) was significantly higher than those of Au_{110}-PEI-PEG_{5000}.siFAM (4.98 min, $p < 0.05$) and siFAM (0.46 min, $p < 0.001$). In summary, these results show that the Au_{110}-PEI-PEG_{5000}-AA.siRNA formulation achieved a 13.5 fold increase in systemic exposure of siRNA relative to the naked control.

3.5.3. Tissue distribution

In this study, the tissue distribution of siRNA was analysed *ex vivo* 2 h after i.v. injection of a single dose containing siFAM alone (~1 mg/kg) or siFAM complexed with Au_{110}-PEI-PEG_{5000} or Au_{110}-PEI-PEG_{5000}-AA (WR40) (n = 4 mice per group) (Fig. S14). It is not surprising that free siRNA did not show efficient retention in the excised tissues (< 7% ID/g). In contrast, the siRNA delivered by AuNP formulations was mainly found in the liver (~40% ID/g), tumour (~15% ID/g) and lung (~10% ID/g) (Fig. S14). Although not statistically different ($p > 0.05$), the tumour uptake of the targeted AuNPs tended to be greater versus the untargeted NP implying that the addition of anisamide targeting ligand may further assist the tissue uptake [24].

Table 1
Pharmacokinetic parameters of siFAM alone or formulated with AuNPs following a single intravenous injection. $t_{1/2}$ = half-life, AUC = area under the curve, Vd = volume of distribution, and CL = clearance. Data = mean ± SD (n = 4). ($^{*}p < 0.05$, $^{**}p < 0.01$ and $^{***}p < 0.001$ relative to siFAM).

Group	$t_{1/2}$ (min)	AUC (μg/mL·min)	Vd (mL)	CL mL/(min·g))
siFAM	0.46 ± 0.07	40.15 ± 1.24	0.27 ± 0.04	0.026 ± 0.005
Au_{110}-PEI-PEG_{5000}.siFAM	4.98 ± 0.25**	52.70 ± 2.84*	2.72 ± 0.12**	0.017 ± 0.002*
Au_{110}-PEI-PEG_{5000}-AA.siFAM	6.20 ± 0.30***	61.59 ± 5.4*	2.82 ± 0.22**	0.016 ± 0.004*

3.5.4. In vivo anti-tumour effects

The therapeutic efficacy of Au_{110}-PEI-PEG_{5000}-AA complex (WR40) containing anti-RelA siRNA (~1 mg/kg) in PC-3 xenograft mice was assessed following i.v. administration (n = 4 mice per group) (Fig. 7b). Results show that the Au_{110}-PEI-PEG_{5000}-AA complex containing siRelA significantly ($p < 0.05$) retarded tumour growth relative to Au_{110}-PEI-PEG_{5000}-AA complex containing negative control siRNA and the saline control group. This anti-tumour effect was mainly due to the *RelA* gene knockdown (Fig. S15).

Recently, it has been reported that i.p. injections of anti-RelA siRNA decreased the expression of NF-κB in gastric cancer, enhanced the sensitivity of tumour cells to PTX, and thereby achieved a synergistic therapeutic effect with PTX in tumour bearing mice [31]. Since PTX is also the first line chemotherapeutic for prostate cancer, the rational for the combination of AuNP.siRNA formulation and PTX in prostate cancer therapy was assessed in this study (Fig. 7b). When a combination of the Au_{110}-PEI-PEG_{5000}-AA.siRelA complex and PTX was given to diseased mice, the anti-tumour efficacy was significantly ($p < 0.01$) higher than either of the individual monotherapies (Fig. 7b). This synergistic effect confirmed the hypothesis that the inactivation of NF-κB can enhance the sensitivity of tumour cells to PTX, which is most likely due to the downregulation of anti-apoptosis genes (i.e. Bcl-2 and Bcl-xL) regulated by NF-κB [32] (Figs. 6 and S15). In addition, the combination of the Au_{110}-PEI-PEG_{5000}-AA.siRelA complex and PTX did not induce any significant toxicity (Figs. S11–S13; Table S3), indicating the potential for clinical translation of this combination strategy in the treatment of prostate carcinoma.

4. Discussion

The systemic application of therapeutic siRNAs has been proposed as a promising treatment for prostate cancer [10]. However, the development of siRNA-based therapeutics is significantly restricted by the lack of safe, efficient and controllable delivery vectors. Recently, NPs have been modified with multifunctional groups that can simultaneously enable delivery to target tissues/cells [33–36] and release drugs *via* stimuli-responsive means either extracellularly and/or intracellularly [37–39], in order to achieve personalised and effective therapeutic regimens.

The sigma receptor was earlier detected in the central nervous system of mammals [40] and recently has been found to overexpress in human cancer cell lines and patient tumour tissues [18,19]. Therefore, a variety of delivery NPs modified with the anisamide or anisamide-derived targeting ligands have been developed to deliver nucleic acids in the treatment of cancer [41–47]. As the sigma receptor is also known to be overexpressed on the cell membrane of various human prostate cancer cell lines and patient primary samples [20,48–50], spherical AuNPs were used in this study as a scaffold to produce positively charged anisamide-targeted PEGylated NPs for delivery of siRNA into prostate cancer (Figs. 1–3). The flow cytometry results show a significantly higher level of cellular uptake with Au_{110}-PEI-PEG_{5000}-AA.-siRNA complex in sigma receptor positive cells (Fig. 4a), confirming the receptor-mediated internalisation of anisamide-targeted AuNPs.

It is worth noting that the sigma receptor consists of two main subclasses namely sigma-1 receptor (σ1R) [18] and sigma-2 receptor (σ2R) [19]. NPs targeting σ1R have shown promise and recently, a number of studies have demonstrated the successful application of σ1R in drug delivery for cancer therapy [44–47]. A debate on the role of σ1R as the receptor for targeted drug delivery has been raised, however the tumour-targeting specificity of σ1R cannot be denied in the absence of more conclusive studies [51]. In addition, due to overexpression of σ2R on the cell membrane of various human and mouse tumour cell lines [52–54], it also has potential as a targeting ligand for diagnostic imaging and therapy. Compounds targeting σ2R are currently under investigation for the diagnosis of breast cancer (clinical trial NCT02762110) and for the treatment of Alzheimer's disease (clinical trial NCT02907567). Due to the lack of appropriate pharmacological inhibitors that selectively block the sigma receptors [51], it is difficult to determine whether single subtypes or both are associated with the receptor-mediated internalisation of Au-PEI-PEG-AA, this will be the focus of future work.

Following ligand-receptor mediated internalisation, NPs are normally trapped in endosomes where the pH becomes slightly acidic (~5 to 6). Subsequently, NPs are transported into lysosomes in which the pH drops further (~4.5) and various degradative enzymes may dissociate NP formulations and degrade siRNA. It has been reported by Gilleron and colleagues that a lipid-based NP delivery system (LNP) released siRNA from endosomes into the cytoplasm with low efficiency (1–2%) [55]. In addition, Sahay et al. reported that ~70% of internalised siRNA formulated with LNPs underwent exocytosis from lysosomes [56]. These studies indicate that delivery nanocarriers must efficiently release siRNA from the endosomes or lysosomes, in order to successfully initiate the RNAi machinery in the cytoplasm.

It has been reported that AuNPs with certain shapes (e.g. Au nanoshells and nanocages) can absorb the light in the near-infra red (NIR) to induce photothermal effects that can assist the endosomal escape of siRNA [57]. In addition, modification of AuNPs with functional groups (e.g. pH-sensitive and enzymes-responsive moieties) may also assist the endosomal release of siRNA [12]. For example, PEI is known to be efficiently in facilitating endosomal escape *via* the "proton sponge effect" whereby the acidic pH in endosomes protonates PEI causing an increase in osmotic pressure and subsequent membrane rupture [58]. In this study, the confocal data demonstrates that Au_{110}-PEI-PEG_{5000}-AA was able to facilitate the intracellular trafficking of siRNA from the endosomes/lysosomes into the endoplasm within 4 h (Fig. 4b), indicating the role of anisamide-targeted AuNPs in promoting endosomal/lysosomal escape of nucleic acids via PEI-mediated "proton sponge effect".

The incorporation of PEG (PEGylation) into NPs is known to prevent aggregation and adsorption of blood components (i.e. serum proteins) [59] and therefore has become one of the most efficient approaches to improve the half-life of NPs in systemic circulation [60]. The circulation time of PEGylated NPs is influenced by the PEG *Mw* (proportional to the chain length), increases in circulation times of ~4, 7 and 17 min have been reported for micelles incorporating 5, 10, and 20 kDa of PEG, respectively [61]. For PEGylated liposomes, conflicting effects have been reported. In one study increased circulation was achieved when the PEG *Mw* was increased from 750 Da to 5 kDa [62], in contrast another study found negligible effects with PEG *Mw* ranging from 350 Da to 2 kDa [63] suggesting that longer PEG lengths are required to prolong *in vivo* exposure.

As described in Fig. 3c, AuNP formulations with longer PEGylation (*Mw* = 7500) demonstrated better *in vitro* stability compared to shorter

PEGylation (Mw = 3500 and 5000). However, longer PEGylation (Mw = 7500) negatively affected the siRNA binding efficiency in comparison to shorter PEGylation (Mw = 3500 and 5000) (Fig. S8). Under the experimental conditions used in this study, Au_{110}-PEI-PEG_{5000}-AA could efficiently complex siRNA achieving a formulation with favourable physicochemical properties, therefore, the pharmacokinetic profile of this construct was evaluated. Consequently, Au_{110}-PEI-PEG_{5000}-AA significantly increased the systemic exposure of siRNA relative to the naked control (Table 1 and Fig. 7a), confirming the role of PEGylation in shielding the surface charge and prolonging blood circulation.

It is known that the leaky blood vessels in solid tumours provide access to circulating NPs with particle size < 500 nm *via* the "enhanced penetration and retention" (EPR) effect [64]. However, NPs above 100 nm are generally recognised by the MPS (e.g. liver Kupffer cells) [65]. In addition, positively charged NPs, due to non-specific adsorption of serum proteins, may be entrapped in the lung [65]. It has been reported that the majority of drugs delivered by NPs was found inside the liver, lung and spleen [66] and in contrast, minimal drug distribution was observed in tumours [e.g. < 5% of injection dose (ID)/g] [67,68]. The concept of prolonged systemic exposure of siRNA, to promote tumour distribution, by anisamide-targeted AuNPs was subsequently evaluated (Fig. S14). As a result, anisamide-targeted PEGylated AuNPs with an average hydrodynamic diameter (~130 nm) significantly achieved the accumulation of siRNA in the tumour (~15% ID/g) in comparison with previous studies (< 5% ID/g) [67,68]. Following the tumour accumulation, the anisamide-targeted AuNP.siRNA complexes can potentially associate with sigma receptors and enter into cells by receptor-mediated endocytosis.

The nuclear factor κ-B [NF-κB, a combination of five gene products (RelA, RelB, c-Rel, NF-κB1 and NF-κB2 [22])] is a substantially investigated transcription factor that has been implicated in cell proliferation, angiogenesis and metastasis of prostate carcinoma, therefore presenting a promising target for cancer therapy [69]. Indeed, siRNA-based blockage of NF-κB has resulted in *in vitro* and *in vivo* anti-proliferative and anti-metastasis effects [70–73]. In addition, when the NF-κB transcription factor is activated, tumour cells are known to become resistant to conventional chemo- and radiotherapy [69]. Recently, a combination strategy has been applied to re-sensitise cancer cells to chemotherapeutics by suppressing the NF-κB signalling pathway [74]. It has also been reported that transfection of anti-RelA siRNA improved the sensitivity of PC-3 cells to chemotherapeutics (docetaxel and cisplatin) [75], due most likely to the downregulation of anti-apoptosis genes such as Bcl-2 and Bcl-xL (these are NF-κB downstream genes) [32]. In this study, anisamide-targeted AuNP complexation containing siRelA significantly slowed down the tumour growth in PC-3 derived xenografted mice relative to the saline control (Fig. 7b). In addition, when combined with Paclitaxel (PTX, an alkaloid with microtubule-targeting capacity, widely utilised to treat a variety of cancers [28]), the downregulation of NF-κB mediated by siRelA using Au_{110}-PEI-PEG_{5000}-AA achieved a synergistic anti-proliferative effect in comparison to either PTX or Au_{110}-PEI-PEG_{5000}-AA.siRNA alone (Figs. 5, 6 and S10), indicating the therapeutic potential of this combination strategy in the treatment of prostate cancer.

It is worth noting that although AuNPs are generally considered non-toxic and biocompatible, they are not easily metabolised and may thus cause unexpected *in vivo* toxicity [76,77]. Results of Fig. S14 suggest that Au_{110}-PEI-PEG_{5000} or Au_{110}-PEI-PEG_{5000}-AA was likely found inside a range of organs (mainly the liver). Although no significant signs of systemic toxicity were recorded by AuNPs (Figs. S11–S13; Table S3), future work will be carried out to evaluate *in vivo* effects such as accumulation in healthy tissues and renal clearance [76–78].

5. Conclusions

A range of positively charged anisamide-targeted PEGylated AuNPs (namely Au-PEI-PEG-AA) were developed for delivery of therapeutic siRNA in the treatment of prostate carcinoma. One of these Au-PEI-PEG-AA, namely Au_{110}-PEI-PEG_{5000}-AA could effectively complex siRNA *via* the electrostatic interaction, and the resultant complexation (Au_{110}-PEI-PEG_{5000}-AA.siRNA) demonstrated favourable particle size, surface charge, and stability. The *in vitro* studies show cell specific internalisation indicating the function of the anisamide targeting ligand. Following intravenous administration the tumour reduction was reflected in the siRNA-mediated knockdown of NF-κB. More importantly, a synergistic therapeutic effect was promoted by a corresponding downregulation of target gene in combination with chemotherapeutics, without showing significant toxicity. These results imply that the anisamide-targeted AuNP vector provides a promising strategy for combination therapy in the treatment of prostate cancer.

Conflicts of interest

There are no conflicts of interest to declare.

Acknowledgement

This work is supported by the Outstanding Youth Foundation from the Department of Science and Technology, Jilin Province, China (20170520046JH); the Start-Up Research Grant Program from Jilin University (451170301168, 451160102052, 419080500667); the Fundamental Research Funds for the Central Universities, China.

Appendix A. Supplementary material

Supplementary data to this article can be found online at https://doi.org/10.1016/j.ejpb.2019.02.013.

References

[1] F. Bray, J. Ferlay, I. Soerjomataram, R.L. Siegel, L.A. Torre, A. Jemal, Global cancer statistics 2018: GLOBOCAN estimates of incidence and mortality worldwide for 36 cancers in 185 countries, CA Cancer J. Clin. 68 (2018) 394–424.
[2] K.A. Fitzgerald, J.C. Evans, J. McCarthy, J. Guo, M. Prencipe, M. Kearney, W.R. Watson, C.M. O'Driscoll, The role of transcription factors in prostate cancer and potential for future RNA interference therapy, Expert Opin. Ther. Targets 18 (2014) 633–649.
[3] S.M. Elbashir, J. Harborth, W. Lendeckel, A. Yalcin, K. Weber, T. Tuschl, Duplexes of 21-nucleotide RNAs mediate RNA interference in cultured mammalian cells, Nature 411 (2001) 494–498.
[4] J. Guo, L. Bourre, D.M. Soden, G.C. O'Sullivan, C. O'Driscoll, Can non-viral technologies knockdown the barriers to siRNA delivery and achieve the next generation of cancer therapeutics? Biotechnol. Adv. 29 (2011) 402–417.
[5] Z. Wang, G. Liu, H. Zheng, X. Chen, Rigid nanoparticle-based delivery of anti-cancer siRNA: challenges and opportunities, Biotechnol. Adv. 32 (2014) 831–843.
[6] H.J. Kim, A. Kim, K. Miyata, K. Kataoka, Recent progress in development of siRNA delivery vehicles for cancer therapy, Adv. Drug Deliv. Rev. 104 (2016) 61–77.
[7] P. Resnier, T. Montier, V. Mathieu, J.P. Benoit, C. Passirani, A review of the current status of siRNA nanomedicines in the treatment of cancer, Biomaterials 34 (2013) 6429–6443.
[8] J. Guo, M.R. Cahill, S.L. McKenna, C.M. O'Driscoll, Biomimetic nanoparticles for siRNA delivery in the treatment of leukaemia, Biotechnol. Adv. 32 (2014) 1396–1409.
[9] H. Uludag, B. Landry, J. Valencia-Serna, K.C. Remant-Bahadur, D. Meneksedag-Erol, Current attempts to implement siRNA-based RNAi in leukemia models, Drug Discovery Today 21 (2016) 1412–1420.
[10] J. Guo, J.C. Evans, C.M. O'Driscoll, Delivering RNAi therapeutics with non-viral technology: a promising strategy for prostate cancer? Trends Mol. Med. 19 (2013) 250–261.
[11] A. Wittrup, J. Lieberman, Knocking down disease: a progress report on siRNA therapeutics, Nat. Rev. Genet. 16 (2015) 543–552.
[12] J. Guo, K. Rahme, K.A. Fizgerald, J.D. Holmes, C.M. O'Driscoll, Biomimetic gold nanocomplexes for gene knockdown: Will gold deliver dividends for small interfering RNA nanomedicines? Nano Res. 8 (2015) 3110–3140.
[13] J. Guo, M.J. Armstrong, C.M. O'Driscoll, J.D. Holmes, K. Rahme, Positively charged, surfactant-free gold nanoparticles for nucleic acid delivery, RSC Adv. 5 (2015) 17862–17871.

[14] K.A. Fizgerald, K. Rahme, J. Guo, J.D. Holmes, C.M. O'Driscoll, Anisamide-targeted gold nanoparticles for siRNA delivery in prostate cancer – synthesis, physicochemical characterisation and in vitro evaluation, J. Mater. Chem. B 4 (2016) 2242–2252.
[15] K. Rahme, J. Guo, J.D. Holmes, C.M. O'Driscoll, Evaluation of the physicochemical properties and the biocompatibility of polyethylene glycol-conjugated gold nanoparticles: a formulation strategy for siRNA delivery, Colloids surf. B, Biointerf. 135 (2015) 604–612.
[16] S. Mishra, P. Webster, M.E. Davis, PEGylation significantly affects cellular uptake and intracellular trafficking of non-viral gene delivery particles, Eur. J. Cell Biol. 83 (2004) 97–111.
[17] J. Guo, C.M. O'Driscoll, J.D. Holmes, K. Rahme, Bioconjugated gold nanoparticles enhance cellular uptake: a proof of concept study for siRNA delivery in prostate cancer cells, Int. J. Pharm. 509 (2016) 16–27.
[18] F.J. Kim, C.M. Maher, Sigma1 pharmacology in the context of cancer, Handb. Exp. Pharmacol. 244 (2017) 237–308.
[19] C.G. Rousseaux, S.F. Greene, Sigma receptors [sigmaRs]: biology in normal and diseased states, J. Recept Signal Transduct. Res. (2015) 1–62.
[20] R. Banerjee, P. Tyagi, S. Li, L. Huang, Anisamide-targeted stealth liposomes: a potent carrier for targeting doxorubicin to human prostate cancer cells, Int. J. Cancer 112 (2004) 693–700.
[21] J. Guo, J.R. Ogier, S. Desgranges, R. Darcy, C. O'Driscoll, Anisamide-targeted cyclodextrin nanoparticles for siRNA delivery to prostate tumours in mice, Biomaterials 33 (2012) 7775–7784.
[22] X. Dolcet, D. Llobet, J. Pallares, X. Matias-Guiu, NF-kB in development and progression of human cancer, Virchows Arch. 446 (2005) 475–482.
[23] B.M. Godinho, J.R. Ogier, A. Quinlan, R. Darcy, B.T. Griffin, J.F. Cryan, C.M. O'Driscoll, PEGylated cyclodextrins as novel siRNA nanosystems: correlations between polyethylene glycol length and nanoparticle stability, Int. J. Pharm. 473 (2014) 105–112.
[24] S.D. Li, Y.C. Chen, M.J. Hackett, L. Huang, Tumor-targeted delivery of siRNA by self-assembled nanoparticles, Mol. Ther. 16 (2008) 163–169.
[25] W.T. Godbey, K.K. Wu, A.G. Mikos, Poly(ethylenimine) and its role in gene delivery, J. Control. Release 60 (1999) 149–160.
[26] S. Son, R. Namgung, J. Kim, K. Singha, W.J. Kim, Bioreducible polymers for gene silencing and delivery, Acc. Chem. Res. 45 (2012) 1100–1112.
[27] S.D. Li, S. Chono, L. Huang, Efficient gene silencing in metastatic tumor by siRNA formulated in surface-modified nanoparticles, J. Control. Release 126 (2008) 77–84.
[28] T.M. Mekhail, M. Markman, Paclitaxel in cancer therapy, Expert Opin. Pharmacother. 3 (2002) 755–766.
[29] K.A. Whitehead, R. Langer, D.G. Anderson, Knocking down barriers: advances in siRNA delivery, Nat. Rev. Drug Discov. 8 (2009) 129–138.
[30] J. Guo, K.A. Fisher, R. Darcy, J.F. Cryan, C. O'Driscoll, Therapeutic targeting in the silent era: advances in non-viral siRNA delivery, Mol. BioSyst. 6 (2010) 1143–1161.
[31] M. Inoue, S. Matsumoto, H. Saito, S. Tsujitani, M. Ikeguchi, Intraperitoneal administration of a small interfering RNA targeting nuclear factor-kappa B with paclitaxel successfully prolongs the survival of xenograft model mice with peritoneal metastasis of gastric cancer, Int. J. Cancer 123 (2008) 2696–2701.
[32] C.Y. Wang, J.C. Cusack Jr., R. Liu, A.S. Baldwin Jr., Control of inducible chemoresistance: enhanced anti-tumor therapy through increased apoptosis by inhibition of NF-kappaB, Nat. Med. 5 (1999) 412–417.
[33] R. Prades, S. Guerrero, E. Araya, C. Molina, E. Salas, E. Zurita, J. Selva, G. Egea, C. Lopez-Iglesias, M. Teixido, M.J. Kogan, E. Giralt, Delivery of gold nanoparticles to the brain by conjugation with a peptide that recognizes the transferrin receptor, Biomaterials 33 (2012) 7194–7205.
[34] Y. Yi, H.J. Kim, P. Mi, M. Zheng, H. Takemoto, K. Toh, B.S. Kim, K. Hayashi, M. Naito, Y. Matsumoto, K. Miyata, K. Kataoka, Targeted systemic delivery of siRNA to cervical cancer model using cyclic RGD-installed unimer polyion complex-assembled gold nanoparticles, J. Control. Release 244 (2016) 247–256.
[35] R. Deng, N. Shen, Y. Yang, H. Yu, S. Xu, Y.W. Yang, S. Liu, K. Meguellati, F. Yan, Targeting epigenetic pathway with gold nanoparticles for acute myeloid leukemia therapy, Biomaterials 167 (2018) 80–90.
[36] J. Guo, X. Luan, Z. Cong, Y. Sun, L. Wang, S.L. McKenna, M.R. Cahill, C.M. O'Driscoll, The potential for clinical translation of antibody-targeted nanoparticles in the treatment of acute myeloid leukaemia, J. Control. Release 286 (2018) 154–166.
[37] L. Han, J. Zhao, X. Zhang, W. Cao, X. Hu, G. Zou, X. Duan, X.J. Liang, Enhanced siRNA delivery and silencing gold-chitosan nanosystem with surface charge-reversal polymer assembly and good biocompatibility, ACS Nano 6 (2012) 7340–7351.
[38] F. Perche, Y. Yi, L. Hespel, P. Mi, A. Dirisala, H. Cabral, K. Miyata, K. Kataoka, Hydroxychloroquine-conjugated gold nanoparticles for improved siRNA activity, Biomaterials 90 (2016) 62–71.
[39] P. Zhang, C. Wang, J. Zhao, A. Xiao, Q. Shen, L. Li, J. Li, J. Zhang, Q. Min, J. Chen, H.Y. Chen, J.J. Zhu, Near infrared-guided smart nanocarriers for MicroRNA-controlled release of doxorubicin/siRNA with intracellular ATP as fuel, ACS Nano 10 (2016) 3637–3647.
[40] W.R. Martin, C.G. Eades, J.A. Thompson, R.E. Huppler, P.E. Gilbert, The effects of morphine- and nalorphine- like drugs in the nondependent and morphine-dependent chronic spinal dog, J. Pharmacol. Exp. Ther. 197 (1976) 517–532.
[41] Y. Chen, S.R. Bathula, Q. Yang, L. Huang, Targeted nanoparticles deliver siRNA to melanoma, J. Invest. Dermatol. 130 (2010) 2790–2798.
[42] Y. Wang, H.H. Su, Y. Yang, Y. Hu, L. Zhang, P. Blancafort, L. Huang, Systemic delivery of modified mRNA encoding herpes simplex virus 1 thymidine kinase for targeted cancer gene therapy, Mol. Ther. 21 (2013) 358–367.
[43] B.L. Rodriguez, J.M. Blando, P.D. Lansakara, Y. Kiguchi, J. DiGiovanni, Z. Cui, Antitumor activity of tumor-targeted RNA replicase-based plasmid that expresses interleukin-2 in a murine melanoma model, Mol. Pharm. 10 (2013) 2404–2415.
[44] K.A. Fitzgerald, M. Malhotra, M. Gooding, F. Sallas, J.C. Evans, R. Darcy, C.M. O'Driscoll, A novel, anisamide-targeted cyclodextrin nanoformulation for siRNA delivery to prostate cancer cells expressing the sigma-1 receptor, Int. J. Pharm. 499 (2016) 131–145.
[45] J.C. Evans, M. Malhotra, K.A. Fitzgerald, J. Guo, M.F. Cronin, C.M. Curtin, F.J. O'Brien, R. Darcy, C.M. O'Driscoll, Formulation and evaluation of anisamide-targeted amphiphilic cyclodextrin nanoparticles to promote therapeutic gene silencing in a 3D prostate cancer bone metastases model, Mol. Pharm. 14 (2017) 42–52.
[46] Q. Liu, H. Zhu, K. Tiruthani, L. Shen, F. Chen, K. Gao, X. Zhang, L. Hou, D. Wang, R. Liu, L. Huang, Nanoparticle-mediated trapping of Wnt family member 5A in tumor microenvironments enhances immunotherapy for B-raf proto-oncogene mutant melanoma, ACS Nano 12 (2018) 1250–1261.
[47] W. Song, L. Shen, Y. Wang, Q. Liu, T.J. Goodwin, J. Li, O. Dorosheva, T. Liu, R. Liu, L. Huang, Synergistic and low adverse effect cancer immunotherapy by immunogenic chemotherapy and locally expressed PD-L1 trap, Nat. Commun. 9 (2018) 2237.
[48] C.S. John, B.J. Vilner, B.C. Geyer, T. Moody, W.D. Bowen, Targeting sigma receptor-binding benzamides as in vivo diagnostic and therapeutic agents for human prostate tumors, Cancer Res. 59 (1999) 4578–4583.
[49] A. Marrazzo, J. Fiorito, L. Zappala, O. Prezzavento, S. Ronsisvalle, L. Pasquinucci, G.M. Scoto, R. Bernardini, G. Ronsisvalle, Antiproliferative activity of phenylbutyrate ester of haloperidol metabolite II [(+/-)-MRJF4] in prostate cancer cells, Eur. J. Med. Chem. 46 (2011) 433–438.
[50] N.A. Colabufo, C. Abate, M. Contino, C. Inglese, M. Niso, F. Berardi, R. Perrone, PB183, a sigma receptor ligand, as a potential PET probe for the imaging of prostate adenocarcinoma, Bioorg. Med. Chem. Lett. 18 (2008) 1990–1993.
[51] A. Dasargyri, C.D. Kumin, J.C. Leroux, Targeting nanocarriers with anisamide: fact or artifact? Adv. Mater. 29 (2017).
[52] C. Zeng, S. Vangveravong, J. Xu, K.C. Chang, R.S. Hotchkiss, K.T. Wheeler, D. Shen, Z.P. Zhuang, H.F. Kung, R.H. Mach, Subcellular localization of sigma-2 receptors in breast cancer cells using two-photon and confocal microscopy, Cancer Res. 67 (2007) 6708–6716.
[53] H. Kashiwagi, J.E. McDunn, P.O. Simon Jr., P.S. Goedegebuure, J. Xu, L. Jones, K. Chang, F. Johnston, K. Trinkaus, R.S. Hotchkiss, R.H. Mach, W.G. Hawkins, Selective sigma-2 ligands preferentially bind to pancreatic adenocarcinomas: applications in diagnostic imaging and therapy, Mol. Cancer 6 (2007) 48.
[54] S.U. Mir, I.S. Ahmed, S. Arnold, R.J. Craven, Elevated progesterone receptor membrane component 1/sigma-2 receptor levels in lung tumors and plasma from lung cancer patients, Int. J. Cancer 131 (2012) E1–9.
[55] J. Gilleron, W. Querbes, A. Zeigerer, A. Borodovsky, G. Marsico, U. Schubert, K. Manygoats, S. Seifert, C. Andree, M. Stoter, H. Epstein-Barash, L. Zhang, V. Koteliansky, K. Fitzgerald, E. Fava, M. Bickle, Y. Kalaidzidis, A. Akinc, M. Maier, M. Zerial, Image-based analysis of lipid nanoparticle-mediated siRNA delivery, intracellular trafficking and endosomal escape, Nat. Biotechnol. 31 (2013) 638–646.
[56] G. Sahay, W. Querbes, C. Alabi, A. Eltoukhy, S. Sarkar, C. Zurenko, E. Karagiannis, K. Love, D. Chen, R. Zoncu, Y. Buganim, A. Schroeder, R. Langer, D.G. Anderson, Efficiency of siRNA delivery by lipid nanoparticles is limited by endocytic recycling, Nat. Biotechnol. 31 (2013) 653–658.
[57] J. Guo, K. Rahme, Y. He, L.L. Li, J.D. Holmes, C.M. O'Driscoll, Gold nanoparticles enlighten the future of cancer theranostics, Int. J. Nanomed. 12 (2017) 6131–6152.
[58] G. Creusat, A.S. Rinaldi, E. Weiss, R. Elbaghdadi, J.S. Remy, R. Mulherkar, G. Zuber, Proton sponge trick for pH-sensitive disassembly of polyethylenimine-based siRNA delivery systems, Bioconjug. Chem. 21 (2010) 994–1002.
[59] J.S. Suk, Q. Xu, N. Kim, J. Hanes, L.M. Ensign, PEGylation as a strategy for improving nanoparticle-based drug and gene delivery, Adv. Drug Deliv. Rev. 99 (2016) 28–51.
[60] A. Kolate, D. Baradia, S. Patil, I. Vhora, G. Kore, A. Misra, PEG – a versatile conjugating ligand for drugs and drug delivery systems, J. Control. Release 192 (2014) 67–81.
[61] M. Miteva, K.C. Kirkbride, K.V. Kilchrist, T.A. Werfel, H. Li, C.E. Nelson, M.K. Gupta, T.D. Giorgio, C.L. Duvall, Tuning PEGylation of mixed micelles to overcome intracellular and systemic siRNA delivery barriers, Biomaterials 38 (2015) 97–107.
[62] A. Mori, A.L. Klibanov, V.P. Torchilin, L. Huang, Influence of the steric barrier activity of amphipathic poly(ethyleneglycol) and ganglioside GM1 on the circulation time of liposomes and on the target binding of immunoliposomes in vivo, FEBS Lett. 284 (1991) 263–266.
[63] N. Dos Santos, C. Allen, A.M. Doppen, M. Anantha, K.A. Cox, R.C. Gallagher, G. Karlsson, K. Edwards, G. Kenner, L. Samuels, M.S. Webb, M.B. Bally, Influence of poly(ethylene glycol) grafting density and polymer length on liposomes: relating plasma circulation lifetimes to protein binding, BBA 1768 (2007) 1367–1377.
[64] H. Maeda, H. Nakamura, J. Fang, The EPR effect for macromolecular drug delivery to solid tumors: improvement of tumor uptake, lowering of systemic toxicity, and distinct tumor imaging in vivo, Adv. Drug Deliv. Rev. 65 (2013) 71–79.
[65] W. Li, F.C. Szoka Jr., Lipid-based nanoparticles for nucleic acid delivery, Pharm. Res. 24 (2007) 438–449.
[66] R.M. Schiffelers, H.K. de Wolf, I. van Rooy, G. Storm, Synthetic delivery systems for intravenous administration of nucleic acids, Nanomedicine (Lond.) 2 (2007) 169–181.
[67] H.K. de Wolf, C.J. Snel, F.J. Verbaan, R.M. Schiffelers, W.E. Hennink, G. Storm, Effect of cationic carriers on the pharmacokinetics and tumor localization of nucleic acids after intravenous administration, Int. J. Pharm. 331 (2007) 167–175.

[68] F. Takeshita, Y. Minakuchi, S. Nagahara, K. Honma, H. Sasaki, K. Hirai, T. Teratani, N. Namatame, Y. Yamamoto, K. Hanai, T. Kato, A. Sano, T. Ochiya, Efficient delivery of small interfering RNA to bone-metastatic tumors by using atelocollagen in vivo, Proc. Natl. Acad. Sci. USA 102 (2005) 12177–12182.
[69] V. Baud, M. Karin, Is NF-kappaB a good target for cancer therapy? Hopes and pitfalls, Nat. Rev. Drug Discov. 8 (2009) 33–40.
[70] J. Duan, J. Friedman, L. Nottingham, Z. Chen, G. Ara, C. Van Waes, Nuclear factor-kappaB p65 small interfering RNA or proteasome inhibitor bortezomib sensitizes head and neck squamous cell carcinomas to classic histone deacetylase inhibitors and novel histone deacetylase inhibitor PXD101, Mol. Cancer Ther. 6 (2007) 37–50.
[71] J.C. Evans, J. McCarthy, C. Torres-Fuentes, J.F. Cryan, J. Ogier, R. Darcy, R.W. Watson, C.M. O'Driscoll, Cyclodextrin mediated delivery of NF-kappaB and SRF siRNA reduces the invasion potential of prostate cancer cells in vitro, Gene Ther. 22 (2015) 802–810.
[72] R.A. Ortega, W. Barham, K. Sharman, O. Tikhomirov, T.D. Giorgio, F.E. Yull, Manipulating the NF-kappaB pathway in macrophages using mannosylated, siRNA-delivering nanoparticles can induce immunostimulatory and tumor cytotoxic functions, Int. J. Nanomed. 11 (2016) 2163–2177.
[73] H. Yu, C. Guo, B. Feng, J. Liu, X. Chen, D. Wang, L. Teng, Y. Li, Q. Yin, Z. Zhang, Y. Li, Triple-layered pH-responsive micelleplexes loaded with siRNA and cisplatin prodrug for NF-Kappa B targeted treatment of metastatic breast cancer, Theranostics 6 (2016) 14–27.
[74] P. Godwin, A.M. Baird, S. Heavey, M.P. Barr, K.J. O'Byrne, K. Gately, Targeting nuclear factor-kappa B to overcome resistance to chemotherapy, Front. Oncol. 3 (2013) 120.
[75] Y. Li, F. Ahmed, S. Ali, P.A. Philip, O. Kucuk, F.H. Sarkar, Inactivation of nuclear factor kappaB by soy isoflavone genistein contributes to increased apoptosis induced by chemotherapeutic agents in human cancer cells, Cancer Res. 65 (2005) 6934–6942.
[76] X.D. Zhang, D. Wu, X. Shen, P.X. Liu, F.Y. Fan, S.J. Fan, In vivo renal clearance, biodistribution, toxicity of gold nanoclusters, Biomaterials 33 (2012) 4628–4638.
[77] X.D. Zhang, D. Wu, X. Shen, J. Chen, Y.M. Sun, P.X. Liu, X.J. Liang, Size-dependent radiosensitization of PEG-coated gold nanoparticles for cancer radiation therapy, Biomaterials 33 (2012) 6408–6419.
[78] W.H. De Jong, W.I. Hagens, P. Krystek, M.C. Burger, A.J. Sips, R.E. Geertsma, Particle size-dependent organ distribution of gold nanoparticles after intravenous administration, Biomaterials 29 (2008) 1912–1919.